AD-A195 173 ONE-DIMENSIONAL MODELING OF LIQUID INJECTION IN A REGENERATIVE PROPELLANT GUN(U) ARMY BALLISTIC RESEARCH LAB ABERDEEN PROVING GROUND MD T P COFFEE MAR 88 1/1

UNCLASSIFIED BRL-TR-2897 F/G 19/1 NL

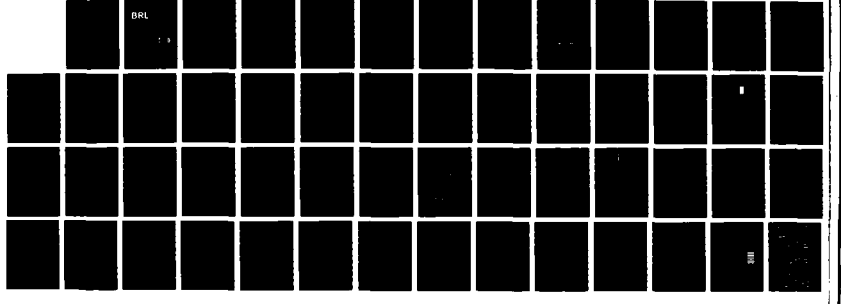

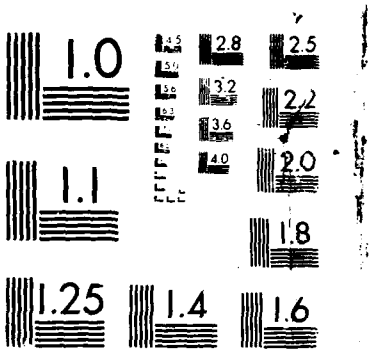

(4)

TECHNICAL REPORT BRL-TR-2897

BRL

1938 – Serving the Army for Fifty Years – 1988

ONE-DIMENSIONAL MODELING OF LIQUID INJECTION IN A REGENERATIVE PROPELLANT GUN

TERENCE P. COFFEE

MARCH 1988

U.S. ARMY LABORATORY COMMAND

BALLISTIC RESEARCH LABORATORY
ABERDEEN PROVING GROUND, MARYLAND

DESTRUCTION NOTICE

Destroy this report when it is no longer needed. DO NOT return it to the originator.

Additional copies of this report may be obtained from the National Technical Information Service, U.S. Department of Commerce, Springfield, VA 22161.

The findings of this report are not to be construed as an official Department of the Army position, unless so designated by other authorized documents.

The use of trade names or manufacturers' names in this report does not constitute indorsement of any commercial product.

nclassified

SECURITY CLASSIFICATION OF THIS PAGE

ADA195173

REPORT DOCUMENTATION PAGE

Form Approved OMB No. 0704-0188

1a. REPORT SECURITY CLASSIFICATION: Unclassified	1b. RESTRICTIVE MARKINGS
2a. SECURITY CLASSIFICATION AUTHORITY	3. DISTRIBUTION/AVAILABILITY OF REPORT
2b. DECLASSIFICATION/DOWNGRADING SCHEDULE	
4. PERFORMING ORGANIZATION REPORT NUMBER(S): BRL-TR-2897	5. MONITORING ORGANIZATION REPORT NUMBER(S)
6a. NAME OF PERFORMING ORGANIZATION: U. S. Army Ballistic Rsch Lab; 6b. OFFICE SYMBOL (If applicable)	7a. NAME OF MONITORING ORGANIZATION
6c. ADDRESS (City, State, and ZIP Code): Aberdeen Proving Ground, MD 21005-5066	7b. ADDRESS (City, State, and ZIP Code)
8a. NAME OF FUNDING/SPONSORING ORGANIZATION; 8b. OFFICE SYMBOL (If applicable)	9. PROCUREMENT INSTRUMENT IDENTIFICATION NUMBER
8c. ADDRESS (City, State, and ZIP Code)	10. SOURCE OF FUNDING NUMBERS: PROGRAM ELEMENT NO. / PROJECT NO. / TASK NO. / WORK UNIT ACCESSION NO.

11. TITLE (Include Security Classification)

ONE-DIMENSIONAL MODELING OF LIQUID INJECTION IN A REGENERATIVE PROPELLANT GUN

12. PERSONAL AUTHOR(S)

Coffee, Terence P.

13a. TYPE OF REPORT	13b. TIME COVERED	14. DATE OF REPORT (Year, Month, Day)	15. PAGE COUNT
TR	FROM _____ TO _____		

16. SUPPLEMENTARY NOTATION

17. COSATI CODES			18. SUBJECT TERMS (Continue on reverse if necessary and identify by block number)
FIELD	GROUP	SUB-GROUP	
20	04		Computational fluid dynamics; discharge coefficient; transient flow; fuel injection; liquid flow; one-dimensional modeling; regenerative gun
19	01	has been	

19. ABSTRACT (Continue on reverse if necessary and identify by block number)

In previous papers, 6-7 the experimental data from a 30-mm regenerative liquid propellant gun was analyzed. The injection of the liquid propellant into the combustion chamber is usually modeled as steady state Bernoulli flow with a fixed discharge coefficient. However, the data analysis indicates that the discharge coefficient increases slowly to approximately a steady value.

To explain this phenomenon, a series of codes have been developed to model the injection process. These are a zero-dimensional (lumped parameter) model (LPIN), a one-dimensional model (ODIN), and a two-dimensional model (MAGIC). For a simple test problem, the three codes are in reasonable agreement.

The two-dimensional code is currently under development, and cannot presently model the large area changes typical of an inline regenerative propellant gun. The zero-

20. DISTRIBUTION/AVAILABILITY OF ABSTRACT	21. ABSTRACT SECURITY CLASSIFICATION
☒ UNCLASSIFIED/UNLIMITED ☐ SAME AS RPT. ☐ DTIC USERS	Unclassified

22a. NAME OF RESPONSIBLE INDIVIDUAL	22b. TELEPHONE (Include Area Code)	22c. OFFICE SYMBOL
Terence P. Coffee	(301) 278-6169	SLCBR-IB-R

DD Form 1473, JUN 86 — Previous editions are obsolete. — SECURITY CLASSIFICATION OF THIS PAGE

Unclassified

19. ABSTRACT (Con't)

dimensional and one-dimensional codes have been applied to an injector resembling that of an actual gun fixture, and agree closely for this case. However, they predict a rapid rise to a steady value. Preliminary indications are that the two-dimensional code will give similar results.

The models do not agree well with the data obtained from the experimental gun firings. Once the two-dimensional model is fully functional, the agreement may improve. But it appears that other phenomena not included in the model are important.

TABLE OF CONTENTS

LIST OF FIGURES

I. INTRODUCTION

Liquid regenerative propellant guns have been proposed as a possible substitute for the traditional solid propellant gun. Morrison et. al. have covered the background and possible applications of liquid propellant guns.[1] Figure 1 shows the design for a typical regenerative gun. The monopropellant is originally in the liquid reservoir. A primer pressurizes the combustion chamber. This starts the regenerative piston moving. Liquid is injected between the moving piston and the fixed central bolt. As the liquid ignites and burns, the rise in pressure accelerates the piston motion and the subsequent fluid injection. The taper at the back of the central bolt slows down the piston at the end of the injection stroke.

Existing liquid propellant gun codes[2-5] involve a number of simplifying assumptions. In this paper the modeling of the injection of the liquid through the orifice between the piston and the bolt is described. In present gun codes, this is usually approximated by steady-state Bernoulli flow. The discharge coefficient is constant throughout the firing cycle. This constant value is often chosen so as to match a desired maximum pressure. However, analysis of data from a 30-mm regenerative gun fired at the BRL indicate that a steady discharge coefficient is not a good approximation.[6-7] When cast in terms of steady-state Bernoulli flow, the discharge coefficient starts small and only gradually builds up to something close to a steady state value. The transient lumped parameter model (LPIN) was described in the latter paper,[7] but the model did not agree well with the experimental data.

Science Applications International Corporation (SAIC) has a contract to develop a two-dimensional model for the injection process. The model is based on an existing code, MAGIC (Modeling Algorithm of a Generic Internal Combustion Engine), developed to model injection and combustion in a diesel engine.[8] This has been modified to model the liquid reservoir in a regenerative liquid propellant gun.[9] In addition,

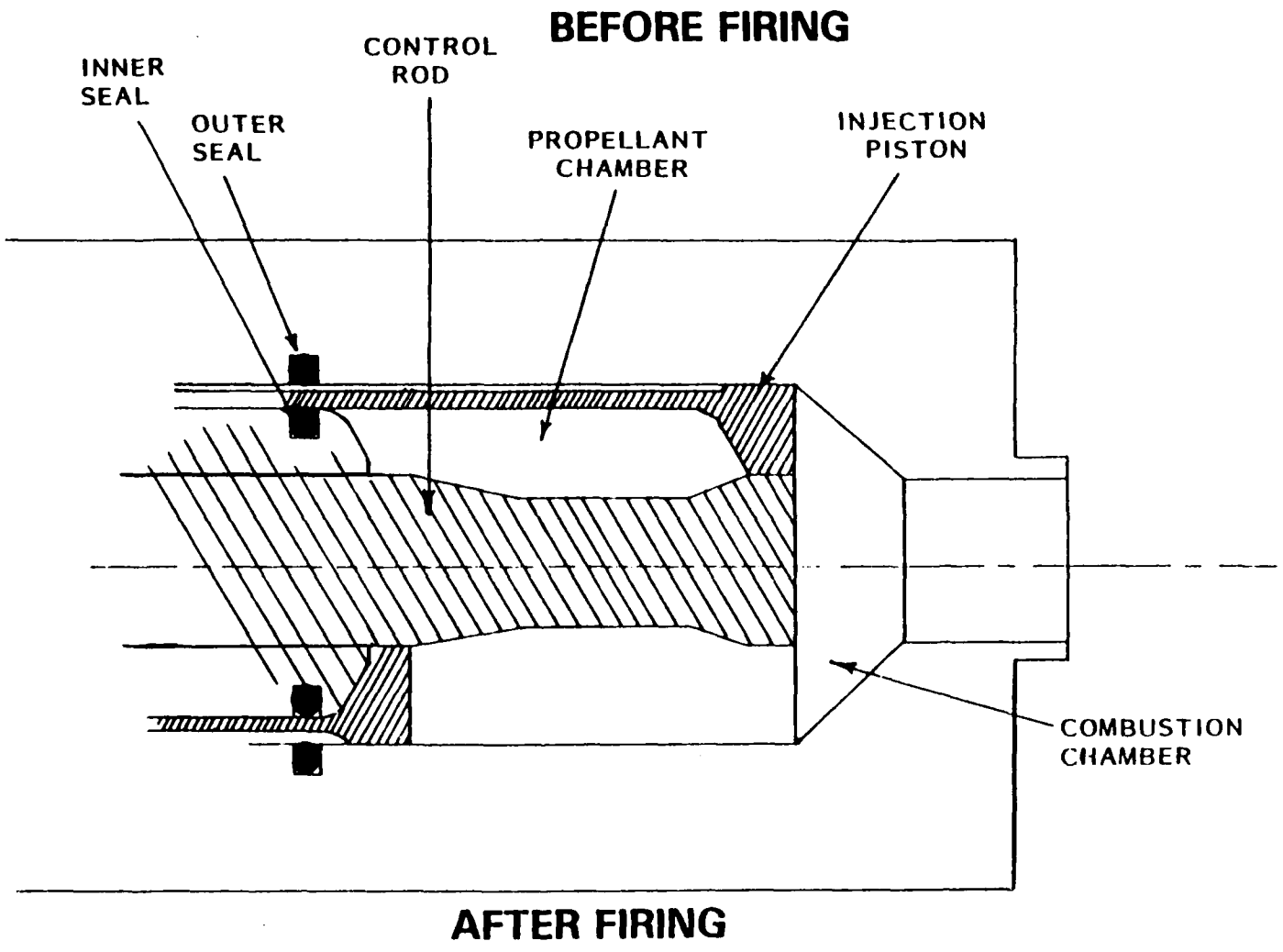

Figure 1. A Regenerative Liquid Propellant Gun with an Annular Piston

the model has been used in the analysis of interior ballistic processes of bulk loaded liquid propellant guns.[10]

The MAGIC code is based on algorithms developed at Los Alamos.[11-12] It is a two-dimensional time-marching code that solves finite-difference approximations of the partial differential equations describing compressible fluid dynamics. A control volume approach has been used with a staggered grid. The grid can vary quite generally in time (ALE - arbitrary Lagrangian-Eulerian mesh). Two temporal differencing options are provided. The first option is an explicit difference scheme whose primary stability limitation is the Courant-Friedrichs-Levy condition. A partially implicit scheme can also be used (ICE method). Centered spatial differencing is utilized for all stress terms in the equations. The spatial advective terms can be approximated by purely centered to full donor cell differencing.

At present there are problems with this code. The primary difficulty is that the code is based on a first order finite difference approximation. The convergence of such a code is very slow. Since discharge coefficients must be predicted, very accurate solutions are required. Even on the BRL CRAY-XMP, a sufficiently fine grid cannot be run, because of both memory and time restrictions.

A secondary problem is that the adaptive gridding algorithm is not general enough. The MAGIC code was designed for use in a simple cylinder with one end moving. The motion of a complicated piston shape moving past a tapered bolt is more difficult. Currently, SAIC is modifying the code to overcome these problems.

Because of these complexities a one-dimensional injection code (ODIN) has been developed. The algorithm is simple enough that the complicated piston and bolt shapes can be readily implemented, and numerical convergence can be easily obtained. Even after the two-dimensional code is fully developed, the one-dimensional code will be

useful for making preliminary runs.

This report discusses the development of the one-dimensional code. For a simple test problem, the code is compared with the MAGIC code. The results are quite similar. When applied to the 30-mm gun problem, the one-dimensional code still gives poor agreement with the experiment. It does agree closely with an earlier lumped parameter injection model (LPIN).

The results suggest that even the two-dimensional model will not be able to predict the injection process. There is apparently some phenomenon we are not properly taking into account.

II. GOVERNING EQUATIONS

The fundamental governing equations are conservation of mass and momentum in the liquid propellant. Preliminary runs with the MAGIC code indicate that the energy increase in the liquid due to the work of compression is negligible, so the energy equation is not implemented. A control volume approach is used. The equations are expressed in integral from for a control element which may be in motion with an arbitrary prescribed velocity U.

The continuity equation is[10]

$$\partial/\partial t \int_{V(t)} \rho dv - \int_{S(t)} \rho(\vec{U} - \vec{u}) \cdot \vec{n}\, dS = 0 \qquad (1)$$

where V is the volume of the element, S is the surface area, $\vec{n}$ is the outward normal vector, ρ is the density, and $\vec{u}$ is the fluid velocity. Although the liquid is almost incompressible, over the large pressure ranges of interest the density changes will be important. The momentum equation is[10]

$$\partial/\partial t \int_{V(t)} \vec{\rho u} dV - \int_{S(t)} \vec{\rho u}(\vec{U} - \vec{u}) \cdot \vec{n} dS + \int_{S(t)} \vec{p n} dS$$

$$- \int_{S(t)} \mu \vec{\nabla u} \vec{n} dS = 0 \qquad (2)$$

where p is the pressure and μ is the dynamic viscosity. The kinematic viscosity has been measured for several propellants as a function of temperature. In this article, HAN1846 at room temperature will be modeled for which the kinematic viscosity is 0.05 stokes.[13] The dynamic viscosity $\mu = \rho\nu$.

The equation of state is[5-7]

$$p = K_1/K_2 \left[(\rho/\rho_o)^{K_2} - 1\right] \qquad (3)$$

where K_1 is the bulk modulus at zero pressure and K_2 is the derivative of the bulk modulus with respect to pressure (bulk modulus $K = K_1 + K_2 p$). For HAN1846, ρ_o=1.43 g/cc,[14] K_1 = 5350 MPa, and K_2 = 9.11.[15]

For the initial conditions the fluid velocity is chosen to be identically zero and the pressure field to be uniform. Other initial conditions have been tried, but if they are not physically reasonable, large oscillations are set up in the solution.

The boundary conditions will be chosen for physical reasons. In the problem of interest, we know the piston velocity and combustion chamber pressure. As seen below, this will translate into specifying the influx velocity and the outflux pressure.

III. FINITE DIFFERENCE APPROXIMATION

The finite difference scheme is taken from the MAGIC code. A staggered grid is used (see Figure 2). Vector quantities are defined on the main grid (solid lines). Scalar quantities are defined at points midway between the main grid values (dotted lines). For flexibility in

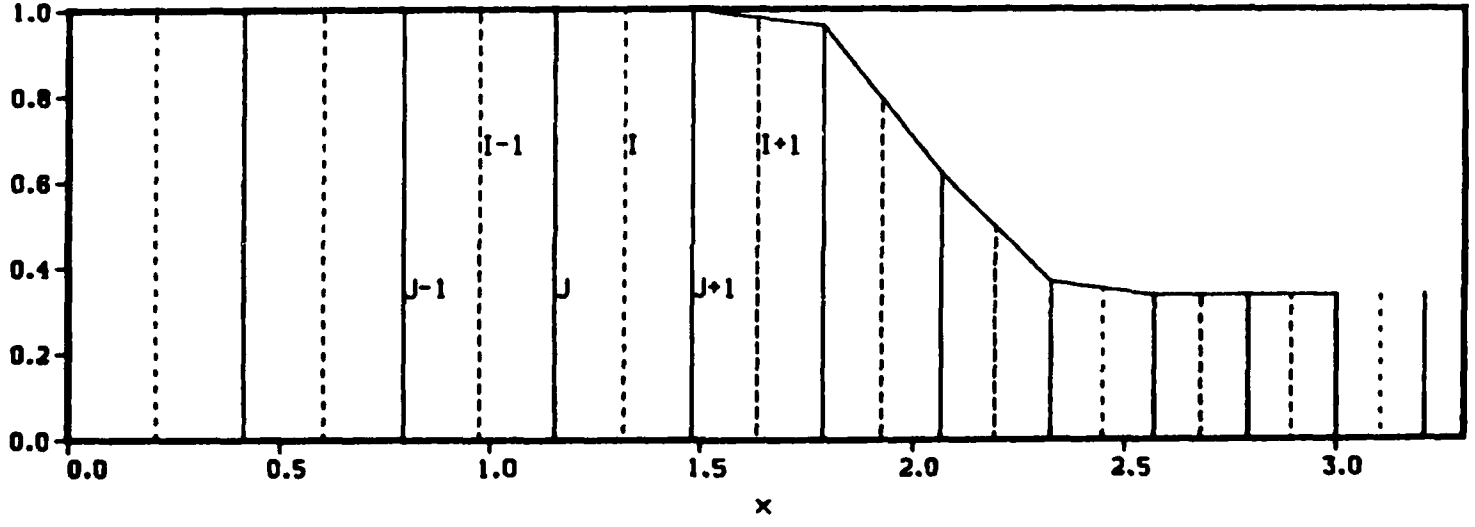

Figure 2. Test Problem with N=11
Vector Grid (line).
Scalar Grid (dot).

implementing boundary conditions, the grid is extended past the physical boundary. Let N-1 be the number of intervals in the region of integration. The vector grid then goes from J=1 to N+1. J=1 is the left boundary, and J=N is the right boundary. The scalar grid goes from I=1 to N. The grid point I is midway between the vector points J and J+1. Unless otherwise stated, it is assumed that I=J. Two different letters are used to distinguish between the vector grid and the scalar grid.

Now consider Eq. (1), the continuity equation, at point I. The control volume for scalar quantities is taken to be from point J to J+1. Let M_I be the mass in the control volume at the present time, and M_I^n be the mass at the next time step. Note that $M_I = \rho_I V_I$. The change in mass is due to mass flux into the control volume minus mass flux out. Using forward time differences,

$$(M_I^n - M_I)/\Delta t = \rho_J(u_J - U_J)A_J - \rho_{J+1}(u_{J+1} - U_{J+1})A_{J+1} \qquad (4)$$

where A is the cross sectional area. The density is not known at the vector grid points, so it must be approximated. To improve the stability of the scheme, upwind differencing is used.[16] The physical rationale is that the density at a point will be primarily determined by the upstream conditions. So let

$$\rho_J = \begin{cases} \rho_{I-1} & u_J \geq 0 \\ \rho_I & u_J < 0 \end{cases} \qquad (5)$$

The density at the new time step is obtained by dividing the mass by the control volume.

Next consider Equation (2), the momentum equation, at point J. The control volume for the vector quantities is taken from point I-1 to I. Then

$$[(M_J u_J)^n - M_J u_J]/\Delta t = -g_o(p_I - p_{I-1})(A_I + A_{I-1})/2$$

$$+ \nu[\rho_I A_I du_I - \rho_{I-1} A_{I-1} du_{I-1} + \rho_J (A_I - A_{I-1}) du_J]$$

$$+ \rho_{I-1} A_{I-1} u_{I-1}(u_{I-1} - U_{I-1}) - \rho_I A_I u_I (u_I - U_I) \qquad (6)$$

The pressure term includes not only the pressure at the left and right sides of the control volume, but also the pressure on the side walls (area = $A_I - A_{I-1}$). This of course only has an effect when the area is changing. The pressure on the side walls is taken to be the average of the pressures at the boundaries of the control volume. The resulting three components are combined into the above form. Similarly, the viscosity term has three components. The velocity derivatives are approximated by central differences.

$$du_I = (u_J - u_{J-1})/(x_J - x_{J-1}) \qquad (7)$$

$$du_J = (u_{J+1} - u_{J-1})/(x_{J+1} - x_{J-1}) \qquad (8)$$

The velocity at the side walls is taken to be zero (no slip condition). The convection terms consist of the momentum flux into the control volume minus the momentum flux out. As before, upwind differencing is used for the convection term.

$$u_I = \begin{cases} u_J & u_J \geq 0 \\ u_{J+1} & u_J < 0 \end{cases} \qquad (9)$$

The mass M_J of the vector control volume must also be computed. This is a weighted average of the masses of the two scalar control volumes.

To maintain stability, the time step will still be constrained by the Courant-Friedrich-Levy (CFL) restriction[17]

$$C = \frac{(|v|+a)\Delta t}{\Delta x} \leq 1 \tag{10}$$

where a is the speed of sound in the liquid, given by

$$a = \sqrt{g_o K/\rho} \tag{11}$$

IV. IMPLEMENTATION

The program was developed to model flow through an annular orifice. The initial shape of the orifice is determined by the central bolt radius and the piston radius. The central bolt consists of straight sections. The piston contains two sections that are arcs of circles.[18] The coordinate system is attached to the piston. The velocity of the back wall is considered known (at J=1). The back wall and center bolt move past the piston. In the actual fixture, the piston is the moving part. For a one-dimensional code, it is irrelevant which part is considered fixed and which part is considered moving.

To specify the initial grid, the number of intervals (N-1) and an expansion factor FAC are entered. A grid is generated such that the largest interval (at the left) is FAC times as large as the smallest interval (at the right). The grid size changes linearly between the boundaries. As time goes on, the back wall moves forward. The velocity of the first grid point, at the back wall, is known. The velocity of the right hand boundary (J=N) is set to zero. The velocities of the other grid points are found by linear interpolation. The intervals at the left are compressed the most, which is why they are chosen to be initially larger. As the grid moves, the radii and cross sectional areas must be recomputed. Normally, a value of FAC=2 was chosen for these calculations.

The influx velocity (J=1) and the outflux pressure (I=N) are user supplied boundary conditions. The pressure and density at the influx boundary (J=1) and the velocity at the outflux boundary (J=N+1) are determined simply by first-order extrapolation. This has been shown to be as stable and accurate as more complicated schemes for at least some problems.[19]

The time step is based on the CFL condition, equation (7). The Courant number C is computed based on the vector control volumes. The velocity u is taken to be the average of the velocities at the boundaries of the control volume. The smallest Courant number is multiplied by a safety factor (usually 0.75) to obtain the next time interval. The partially implicit pressure iteration, which would allow a larger time step, has not been implemented in the one-dimensional code (see discussion below).

The time step integration proceeds in two main stages. First a Lagrangian calculation is performed, assuming that the grid moves with the fluid. The convection terms do not contribute to this part of the calculation. Then the rezone phase takes into account the movement of the fluid with respect to the grid (convection terms).[12] In detail:

1. Compute the size of the next time step Δt based on the CFL condition.

2. Compute the new velocity for the back wall and the outflux pressure (considered known).

3. Interpolate to get the velocity of all the grid points.

4. Find the position of the new grid. Assume the grid velocity over the time interval is the average of the old and the new velocity.

5. Compute the cross sectional areas for the new grid. Compute the control volumes for the new grid.

6. Compute the new mass times fluid velocity based only on the stress terms (pressure and viscosity) in equation (6). Assume for the moment that the grid moves with the fluid (Lagrangian calculation) so the convection terms do not contribute.

7. Compute the mass in the vector control volume by a weighted average of the old masses in the scalar control volumes.

8. Compute the intermediate fluid velocities.

9. Compute the new masses, equation (4), using the updated velocities. Find the new densities using the new values for the control volumes.

10. From the equation of state (3), compute the new pressures.

11. Using the new densities and pressures, update the mass times velocity based on the convection term in equation (6).

12. Compute the mass in the vector control volume by a weighted average of the new masses in the scalar control volumes.

13. Compute the final fluid velocities.

The results can be summarized in terms of the discharge coefficient. The steady state Bernoulli equation is

$$U_n = C_D \sqrt{2g_o\ (p_1 - p_n)/\rho + u_1^2} \qquad (12)$$

where ρ is the average density in the orifice. The subscripts 1 and N denote the boundaries. This equation is derived from the steady state momentum equation (ignoring friction losses). The discharge coefficient

C_D is an empirical number to take into account the loss terms and the error due to the fact that the momentum equation is not at steady state.

V. LUMPED PARAMETER MODEL

In a previous paper,[7] a lumped parameter model was derived for the injection process. The density is assumed to be constant with respect to space in the reservoir. The primary assumption is that the mass flux uA is also constant with respect to space. The gradient is in fact very small, since the liquid is not very compressible. With this assumption, it is possible to integrate the momentum equation and obtain

$$\frac{d(\rho uA)}{dt} = [0.5\rho(u_1^2 - u_n^2) + g_o (p_1 - p_n)]/\int dx/A \qquad (13)$$

The momentum equation is rearranged so the area terms are only on the left side of the equation before the space integration is performed. The integral of the inverse of the cross sectional area is evaluated numerically. In the code, equation (13) is integrated in parallel with the one-dimensional equations.

Like many lumped parameter models, the above is not completely self consistent. Since the density is constant in the reservoir, so is the pressure p_1. The pressure drop is idealized as occurring instantaneously at the outflux boundary. Similarly, the assumption that the mass flux is constant implies that once u_1 is known, the velocity anywhere in the reservoir can be determined by continuity. Again, the change in the mass flux is idealized as occurring instantaneously at the boundary. The above model then in a crude fashion implements the effects of inertia, as there is a delay before a pressure gradient or velocity gradient has an effect on the mass flux out of the reservoir.

VI. PRESSURE WAVES

To begin with, a simple cylinder 3 cm long and with a radius of 1 cm is considered. The outflux pressure is kept fixed at 10 MPa. The back wall is accelerated to 10 cm/s and back to zero in the first 0.002 ms. This creates a pressure wave. Figure 3 shows the pressure profile at two early times. The wave propagates correctly at the speed of sound. At the right hand boundary the pressure wave is inverted. At the left hand boundary it is reflected normally. At later times noise will build up at the trailing edge of the wave. The upwind differencing used in the code is not optimum for tracking a wave front.

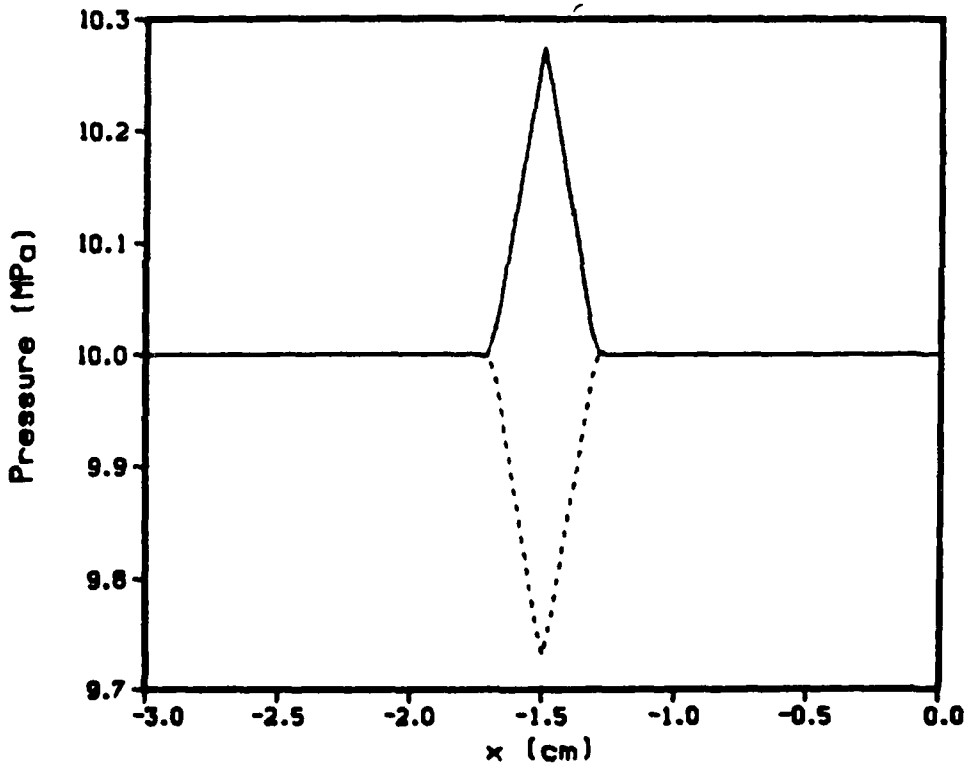

Figure 3. Pressure Wave in a Cylinder
Time = 0.0087 ms (line).
Time = 0.0241 ms (dot).

Now consider why the pressure wave in the code inverts at the right hand boundary. The pressure at the boundary is kept constant, so as the high pressure point approaches the boundary, the pressure gradient becomes steeper. The fluid velocity becomes larger. This relatively large velocity causes a rarefaction wave to form and propagate back into the liquid region.

The proper boundary conditions for the outflow boundary are not obvious. A number of workers have tried to develop non-reflecting boundary conditions. If the boundary is artificial, that is, introduced solely to reduce the size of the region of integration, pressure waves should exit through the outflow boundary. However, for the problems of interest here non-reflecting boundary conditions are not appropriate. At the boundary there is an abrupt area change as the fluid enters the larger combustion chamber. The pressure should drop rapidly to match the combustion chamber pressure, and the behavior of the code at this boundary is reasonable.

Next consider a tube where the radius changes rapidly from 1 cm to 1/3 cm between x = -2.0 cm and x = -1.9 cm. As before, a pressure wave is started at the left boundary. Figure 4 shows the pressure profile after the original wave has traveled 1.5 cm. The interesting point is that the change in area splits the pressure wave. Part of the wave continues forward. As the area decreases, the pressure increases. However, part of the wave is reflected and moves back toward the left. At later times the pressure profile becomes very complex as the waves are repeatedly split.

To see the effects of an sudden increase in area, consider a tube where the radius changes from 1/3 cm to 1 cm between x = -2.0 cm and x = -1.9 cm. Figure 5 shows the profile corresponding to Figure 4. As before, part of the wave continues to the right. As the area increases, the pressure decreases. The reflected part of the wave is inverted. The procedure is that discussed above for the right hand boundary.

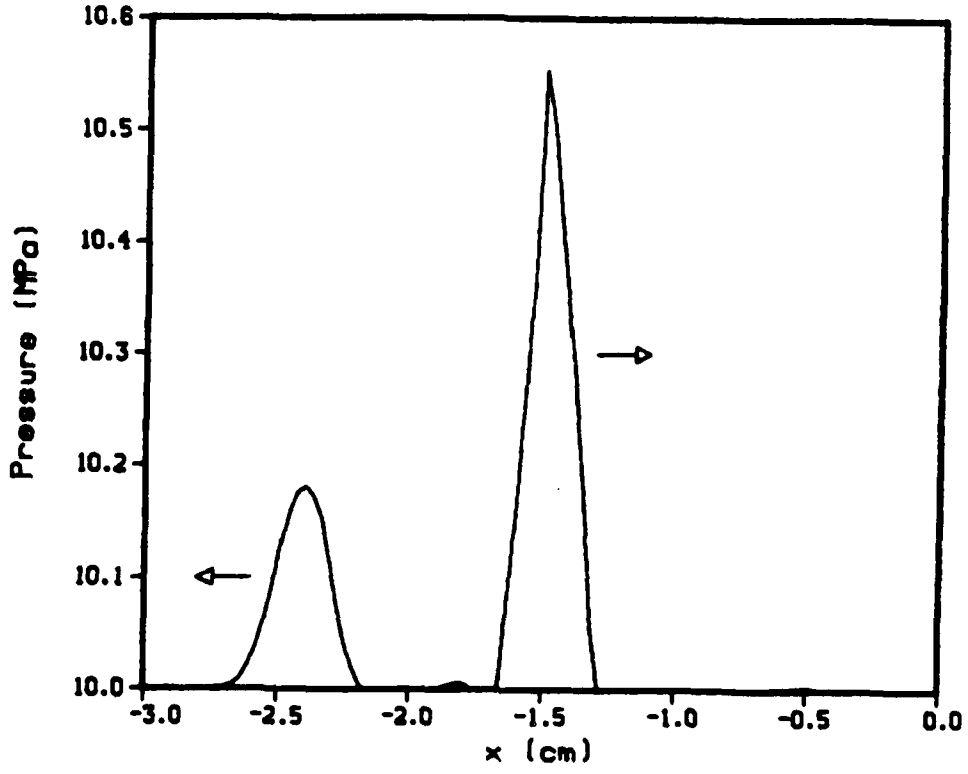

Figure 4. Pressure Wave in a Converging Cylinder
Area decreases at x = -2.0 cm.
Time = 0.0087 ms.

To summarize, the one-dimensional code does track pressure waves properly. An area change will split the pressure wave. This mimics the behavior of a pressure wave at the boundary. An abrupt decrease in area will reflect the wave, and an abrupt increase in area will invert the wave. This is indicative that the boundary conditions are imposed in an appropriate manner.

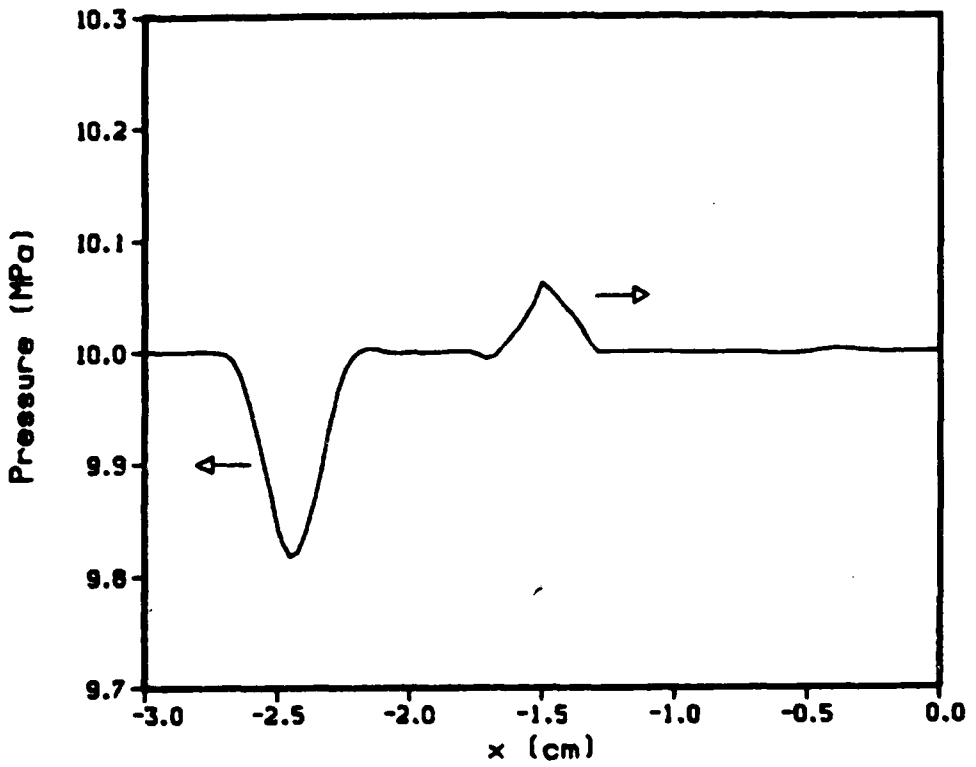

Figure 5. Pressure Wave in a Diverging Cylinder
Area increases at x = -2.0 cm.
Time = 0.0087 ms.

VII. INJECTION FROM A CYLINDER

Again consider a cylinder 3 cm long with a radius of 1 cm. The back wall is accelerated smoothly to 500 cm/s in the first 0.5 ms. The outflux pressure is kept fixed at 10 MPa. The integration is carried out to 1.0 ms. Figure 6 shows the pressure at the back wall as a function of time. As the back wall accelerates, it raises the pressure. There is a time delay until this high pressure region relaxes. After the piston reaches a steady velocity, the pressure oscillates around the steady state value of 10 MPa. The time from a maximum to a minimum value of the pressure matches very closely the time for a sound wave to

travel to the outflux boundary and return. There is very little damping of the pressure oscillations.

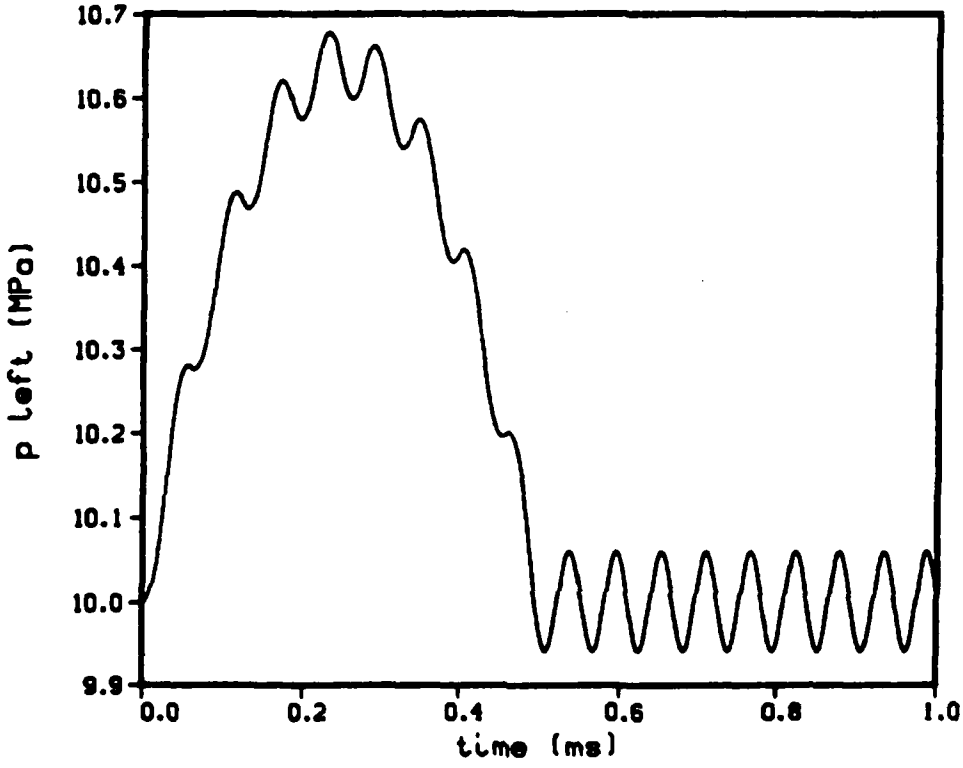

Figure 6. Injection for a Cylinder. Back Wall Pressure.

Figure 7 shows some space profiles of the pressure at the later times. The continuous motion of the back wall has formed a standing wave in the chamber.

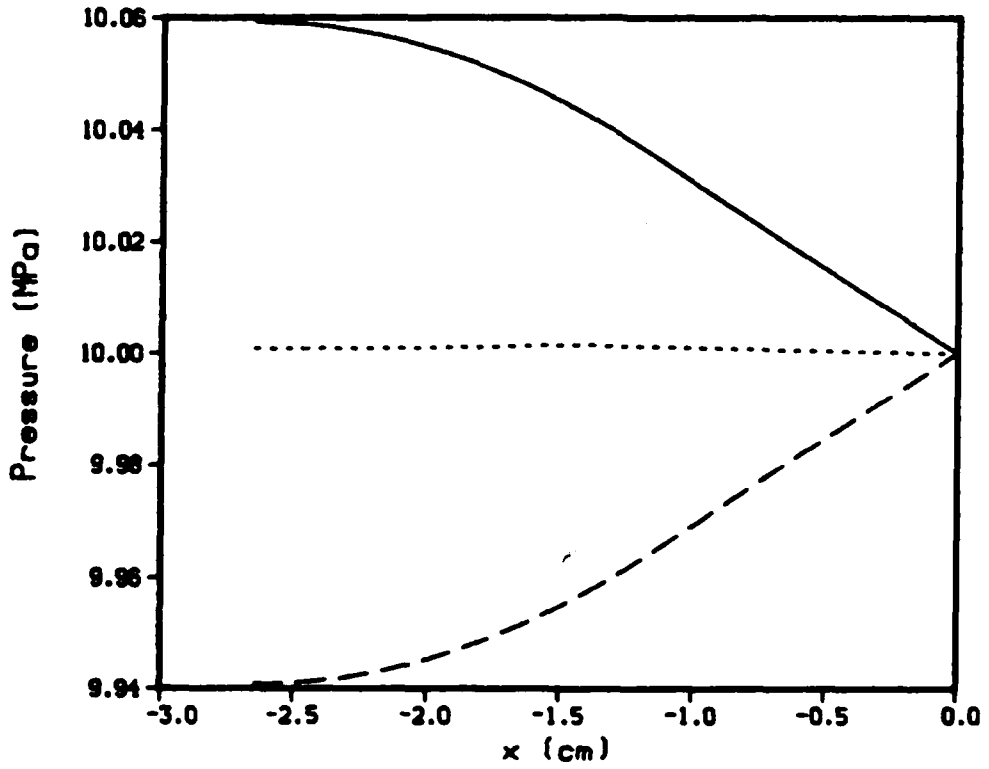

Figure 7. Injection for a Cylinder. Pressure Profiles.
Time = 0.9333 ms (line). Time = 0.9467 ms (dot).
Time = 0.9602 ms (dash).

VIII. TEST PROBLEM

As a more realistic test problem, an orifice with a typical piston shape is considered, but without a central bolt. The orifice is 3 cm long, and the area change from left to right is a factor of 9 (see Figure 8). As above, the back wall is accelerated smoothly to 500 cm/s in the first 0.5 ms. The outflux pressure is kept fixed at 10 MPa. The integration is carried out to 1.0 ms. This relatively simple problem will be used to compare the results of the various codes and for grid checking.

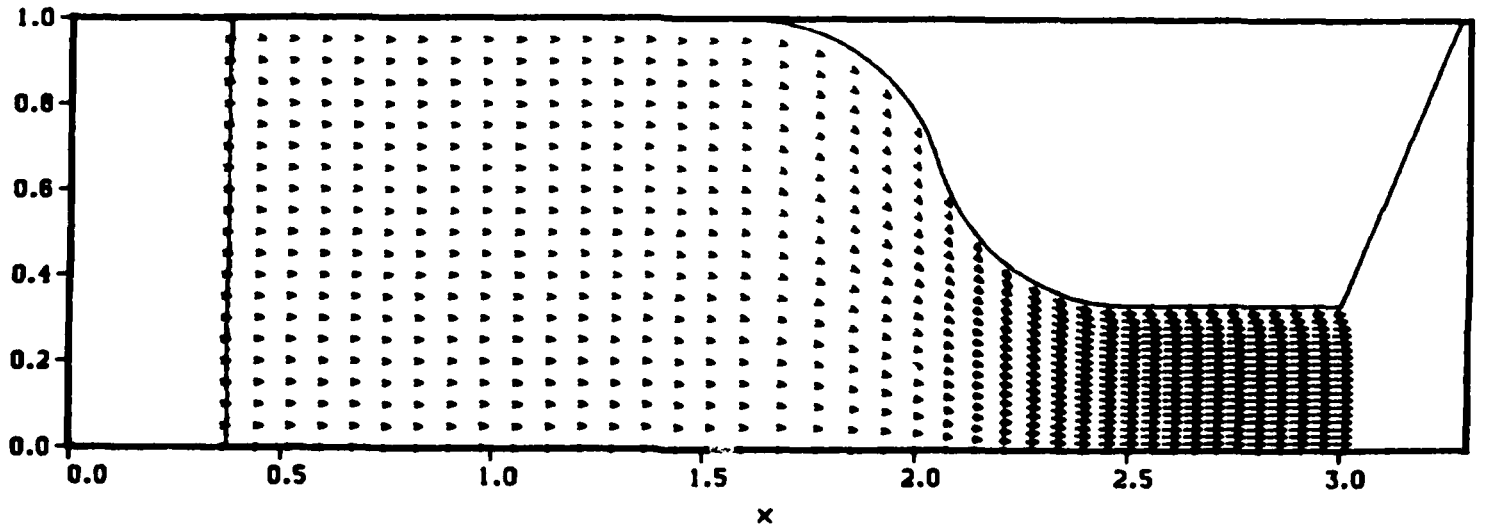

Figure 8. Vector Plot from MAGIC Code, NR=81, NX=314

Table 1 shows a set of runs on the CRAY-XMP for the one-dimensional code. The pressure at the back wall, p_1, at 1.0 ms is given as the most sensitive output value. This pressure primarily determines the discharge coefficient. The problem has essentially converged for 400 grid points. The problem has not reached steady state at 1.0 ms, and the discharge coefficient oscillates around the value one.

Table 1. Grid Check Runs for ODIN Code.

N	p_1 (MPa)	C_D	Run Time min:sec
11	11.76	.861	1
21	12.44	.822	1
41	11.82	.895	2
81	11.73	.917	6
161	11.49	.987	22
241	11.49	.986	47
321	11.46	.997	1:22
401	11.42	1.009	2:07
601	11.44	1.003	4:41
801	11.44	1.000	8:17
1001	11.45	1.007	12:53

The test problem was also solved using the MAGIC code. For simplicity laminar flow was assumed. The number of radial grid points NR was chosen first. The axial spacing is picked so that the grid quadrilaterals are square in the first straight section of the reservoir. The quadrilaterals in the last straight section are rectangles with an aspect ratio of 1.5. The axial grid size decrease smoothly in the converging section. This choice of aspect ratios has been observed to be stable, even for very coarse grids. If large aspect ratios are chosen, the solution will break up. Table 2 shows the grid

check results. The numerical convergence is very slow, and the solution has not converged for the largest grid possible. Part of the problem is the upwind differencing. This generates a numerical viscosity term that depends on the grid spacing.[16] The physical viscosity for room temperature propellant is small (kinematic viscosity = 0.05 stokes),[13] and the numerical viscosity becomes larger than the physical viscosity, even for a fine grid for this simple problem. A more accurate finite difference method appears to be required to predict the discharge coefficients for the more complicated problem of interest (see below).

Table 2. Grid Check Runs for MAGIC Code.

NR	NX	p_1 (MPa)	C_D	Run Time hr:min:sec
6	21	14.94	.540	45
11	40	13.47	.645	3:32
21	79	12.73	.726	22:33
41	158	12.32	.788	2:42:28
61	236	12.16	.816	8:48:08
81	315	12.07	.834	20:55:17

The MAGIC code is partially implicit, and should not be restricted by the Courant condition, equation (10). However, as the time step was increased, the code did many iterations on the implicit pressure iteration to obtain convergence, and the run time did not improve. The code was finally run using a time step only twice the Courant limit. This time step restraint may be due to accuracy considerations. Since the implicit iterations did not seem to be very helpful for this type of problem, it was not implemented in the one-dimensional code.

Figure 8 shows the vector plot generated by the MAGIC code. The solution is smooth and stable. For runs using realistic piston shapes,

such phenomena as flow separation and recirculation have not been observed.

It is more interesting to plot the boundary conditions as a function of time. Figure 9 shows the influx velocity (specified by the user) and the outflux velocities obtained from the different codes. All three codes predict outflux velocities very close to the steady state values (outflux velocity = 9 x influx velocity). A blow up of the outflux velocities (Figure 10) shows oscillations due to the pressure waves.

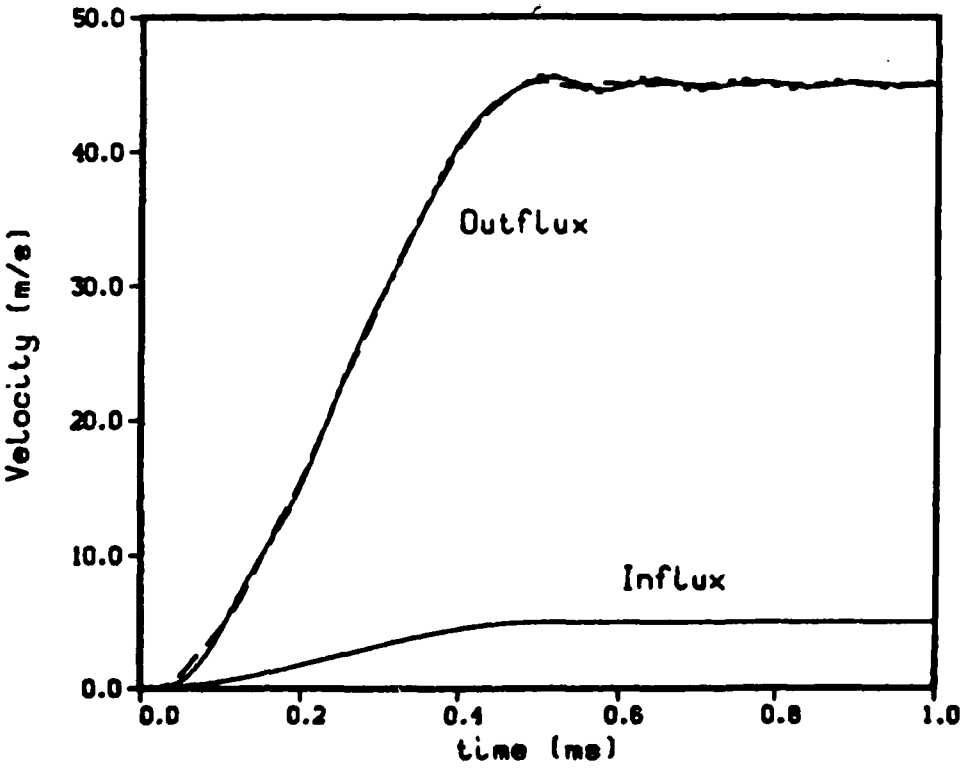

Figure 9. Influx Velocity (Specified) and Outflux Velocities for the Test Problem
MAGIC code (line). ODIN Code (dot).
LPIN (dash).

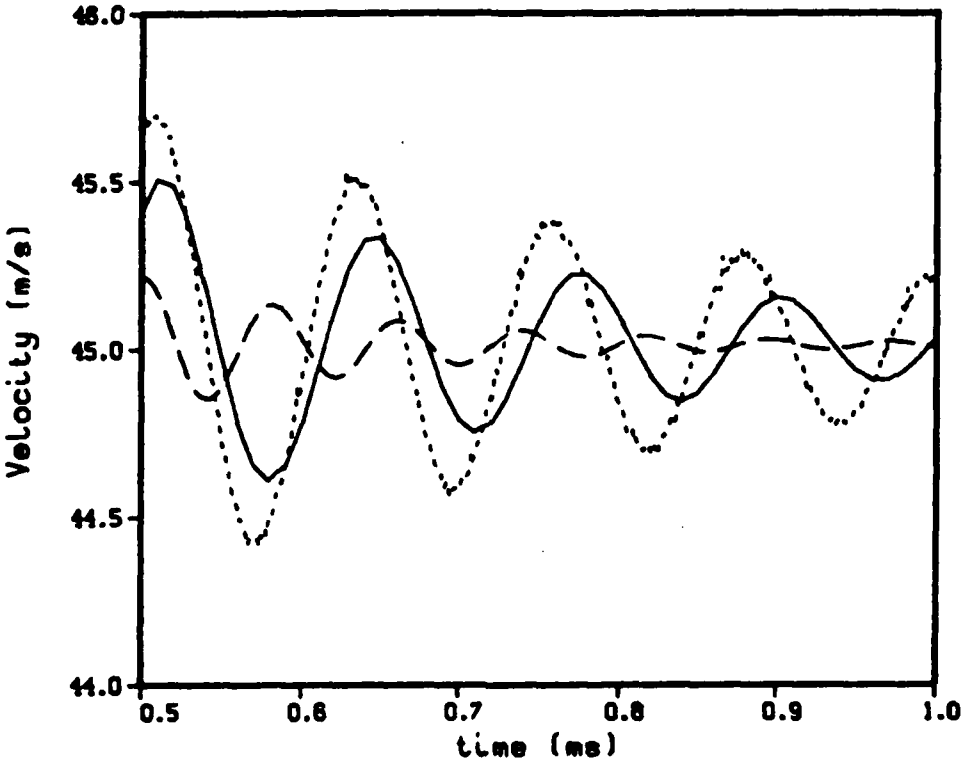

Figure 10. Outflux Velocities for the Test Problem at Later Times
MAGIC Code (line). ODIN Code (dot). LPIN (dash).

Figure 11 shows the pressures at the back wall. The two-dimensional and one-dimensional codes predict qualitatively very similar results. As the back wall accelerates, it raises the pressure. There is a definite time delay until this high pressure region relaxes. The differences are at least partly due to the lack of convergence of the MAGIC code. The lumped parameter code does not predict the initial large overshoot in pressures. Because of the lack of spatial resolution in the mass flux, LPIN predicts a slightly higher mass flux out of the reservoir. Even a slight change in the density of the liquid in the reservoir leads to a large pressure difference. There is a secondary effect due to the fact that LPIN assumes a uniform pressure in the reservoir instead of a pressure gradient. The pressure values primarily determine the computed discharge coefficients (Figure 12).

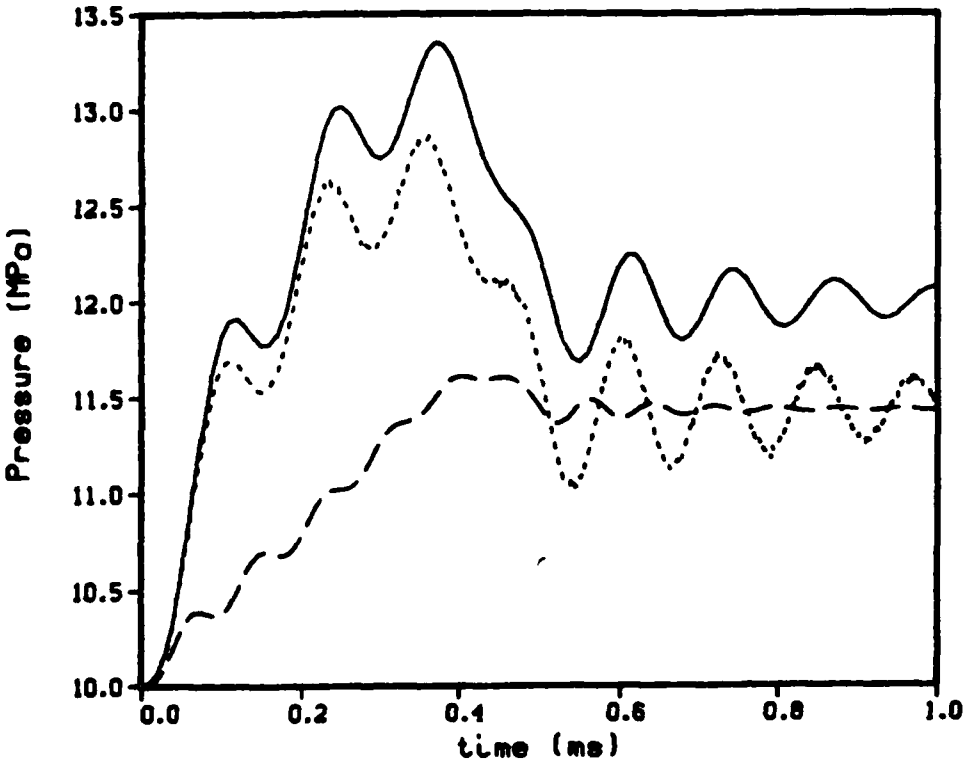

Figure 11. Back Wall Pressures for the Test Problem
MAGIC Code (line). ODIN Code (dot).
LPIN (dash).

The lumped parameter code predicts pressure oscillations, despite the fact that there are no pressure waves or gradients in the model. This is a global phenomenon. Suppose the velocity of the piston is constant, and the liquid pressure is above the steady state pressure. The fluid will be accelerated. As the fluid is injected more rapidly from the reservoir, the pressure will drop. Since the model involves a transient equation, the fluid takes time to slow down, and will be injected more rapidly even after the liquid pressure reaches the steady state pressure. So the liquid pressure will end up below the steady state pressure. The inertia of the system damps these global oscillations fairly rapidly.

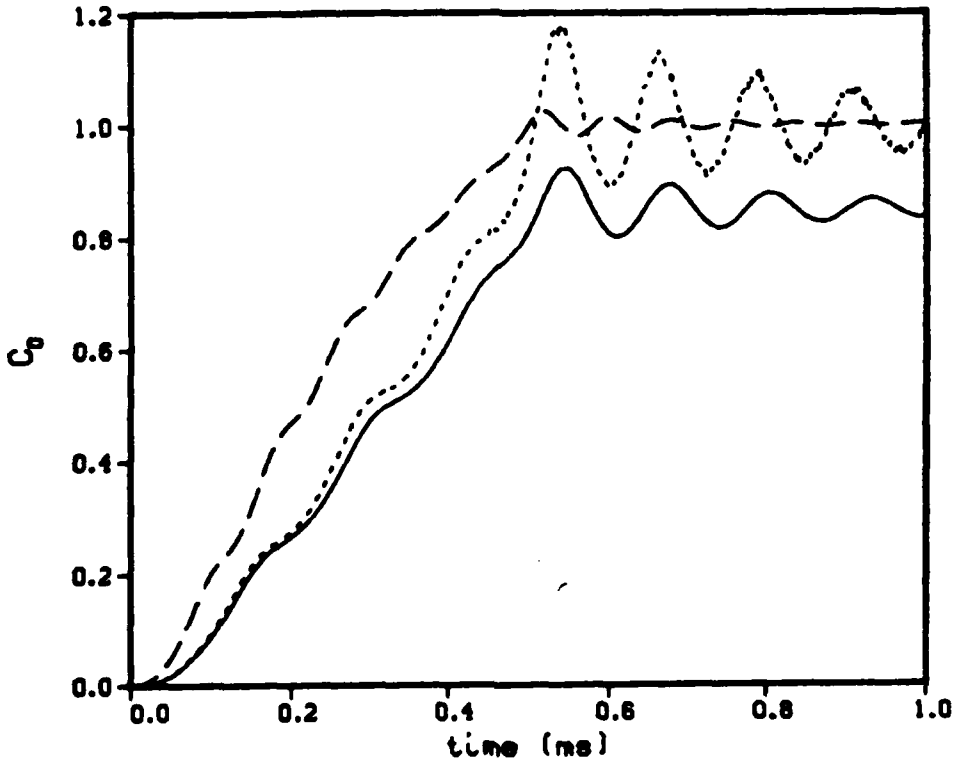

Figure 12. Discharge Coefficients for the Test Problem
MAGIC Code (line). ODIN Code (dot).
LPIN (dash).

The one-dimensional model predicts larger oscillations. These no longer correspond to the time scale of a pressure wave. The change in area causes the pressure surges to be broken up in unpredictable ways. These pressure surges can also partially cancel one another, and the damping is much more rapid than for the case of a cylinder without area changes.

The MAGIC code predicts results very similar to the ODIN code, but the oscillations are damped more rapidly. This is at least partly due to the large numerical viscosity. It may also be partially due to two-dimensional effects (such as wall friction).

IX. 30-MM GUN

Data from the BRL 30-mm gun has been analyzed.[6-7] Here the data from Round 8 is selected. The chamber pressure and the piston travel have been measured. The experimental values are fitted by splines. The chamber pressure fit and the derivative of the piston travel fit are used as input to ODIN. The code computes the back wall pressure and hence the discharge coefficients.

The liquid pressure at the back wall has been measured using mini-transducers. There has been some concern over the accuracy of these transducers. A partial independent check is possible. The injection is caused by the differential piston. At steady state, the liquid pressure should be equal to the chamber pressure times the hydraulic difference (ratio of chamber piston area over liquid reservoir piston area). Figure 13 shows a comparison between the measured liquid pressure and the chamber pressure times the hydraulic difference. The two curves are in reasonable agreement over most of the firing cycle.

The transducer block (at the back of the liquid reservoir) is mounted on Belleville springs. As the piston begins to move, it compresses the liquid, which pushes back on the transducer block and compresses the Belleville springs. This helps the piston to clear the O-ring originally sealing the reservoir and begin the injection process. Very little injection takes place until the springs have been compressed. Rather than include a model of the springs in the inverse code, the assumption is made that the piston, liquid, and springs move as a unit until the springs are fully compressed. This is taken as time zero. At this point the piston is assumed to begin injecting the liquid. The initial conditions are not quite accurate, since the compression of the springs and the injection process are not actually separate phases.

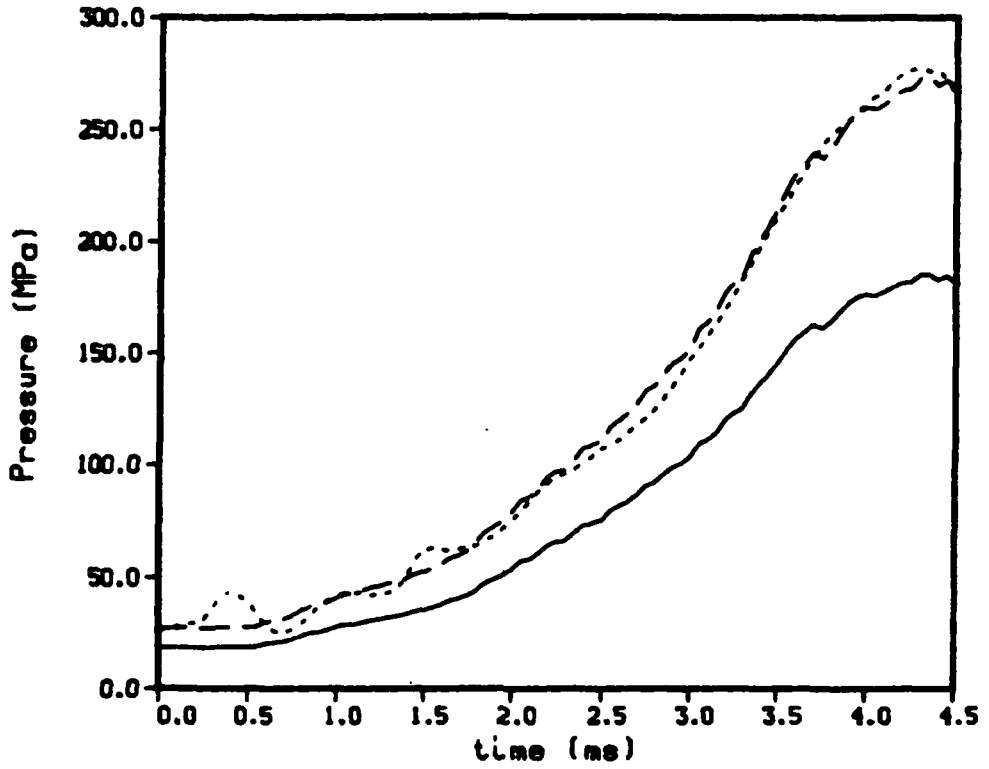

Figure 13. Round 8 Chamber Pressure (line), Measured Liquid Pressure (dot), and Chamber Pressure Times Hydraulic Difference (dash).

Figure 14 shows the central bolt and piston at time zero. The vent area has just begun to open up. Figure 15 shows the outflux velocity. The models predict large oscillations near the start, probably due to the fact that the initial conditions are not accurate. After this, the predicted one-dimensional velocity shows very good agreement, and the predicted zero-dimensional velocity is still reasonably accurate. However, the agreement for the pressures is not as good (Figure 16). Between 1.0 and 2.5 ms, both models predict a liquid pressure well below the values measured. This leads to higher discharge coefficients (Figure 17). The one-dimensional model, like the lumped parameter

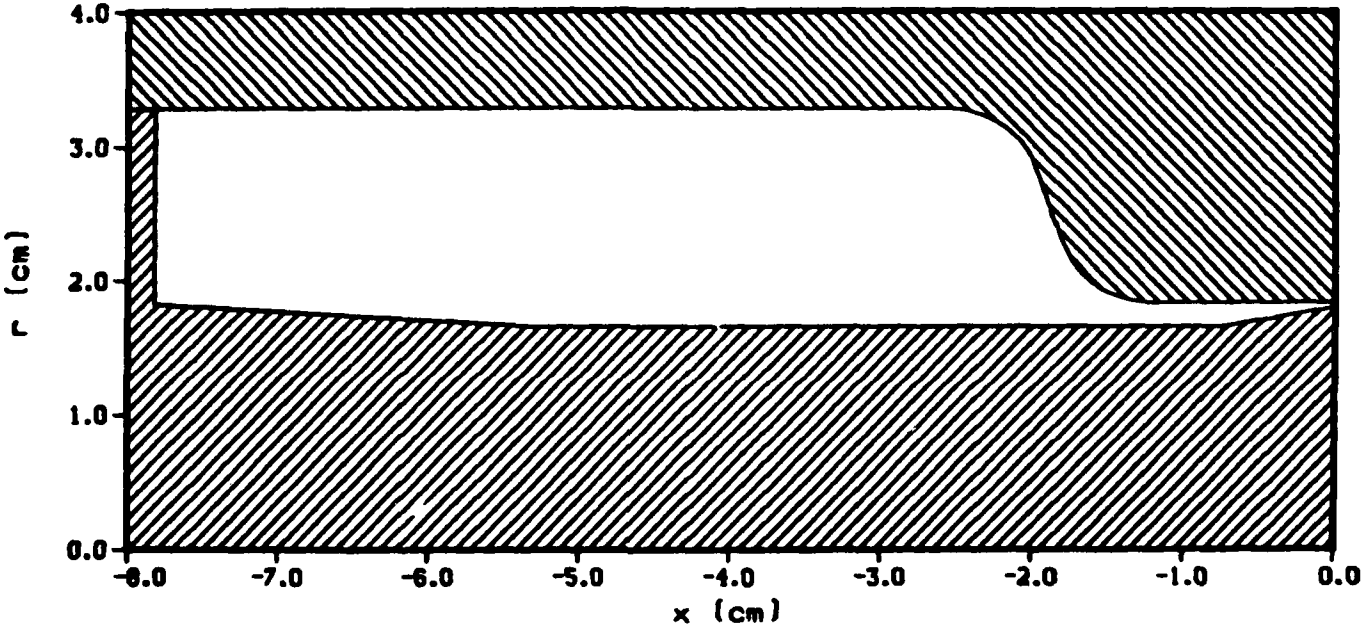

Figure 14. Initial Geometry for the One-Dimensional Model (Round 8)

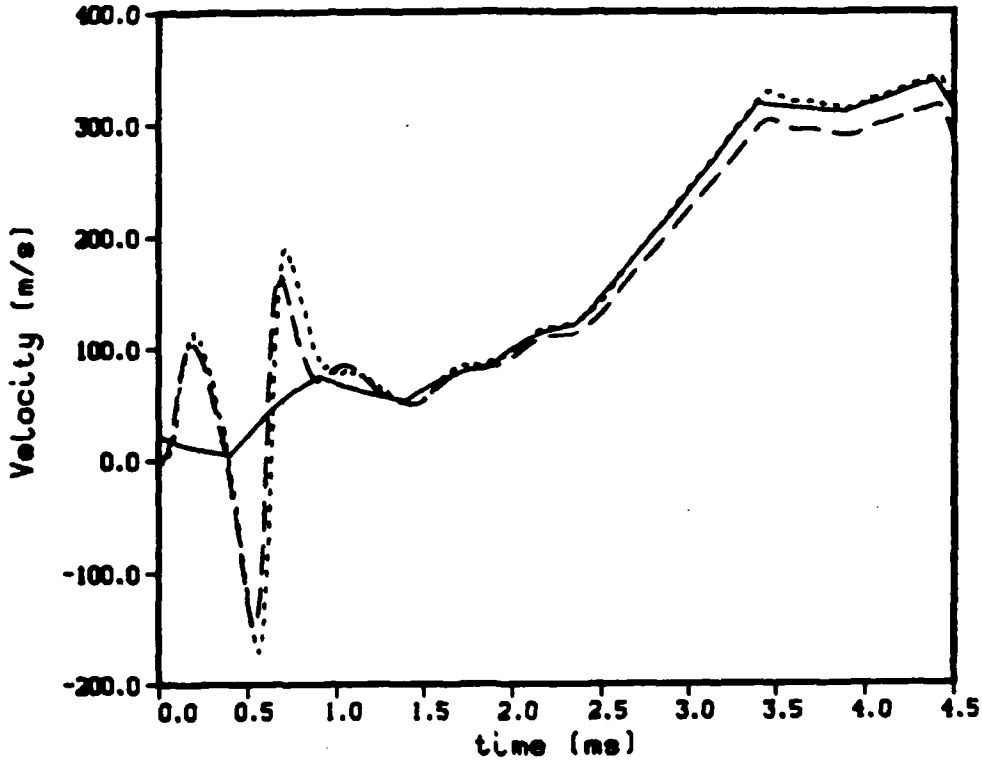

Figure 15. Outflux Fluid Velocities
Round 8 (line). ODIN Code (dot). LPIN Code (dash).

model, shows the discharge coefficient increasing rapidly, rather than the slow increase derived from the experimental data. The one-dimensional model predicts small oscillations in the liquid pressure which lead to large oscillations in the discharge coefficient. These oscillations are not numerical (they are independent of the space and time discretization) and are due to the pressure surges being split by the area changes. In the actual flow turbulence and friction against the walls will tend to damp these oscillations. ODIN and LPIN show much better agreement for the liquid pressure here than for the simpler test problem. Both the back wall velocity and the outflux pressure are more complicated. LPIN alternately overpredicts and underpredicts the outflux. The errors tend to cancel.

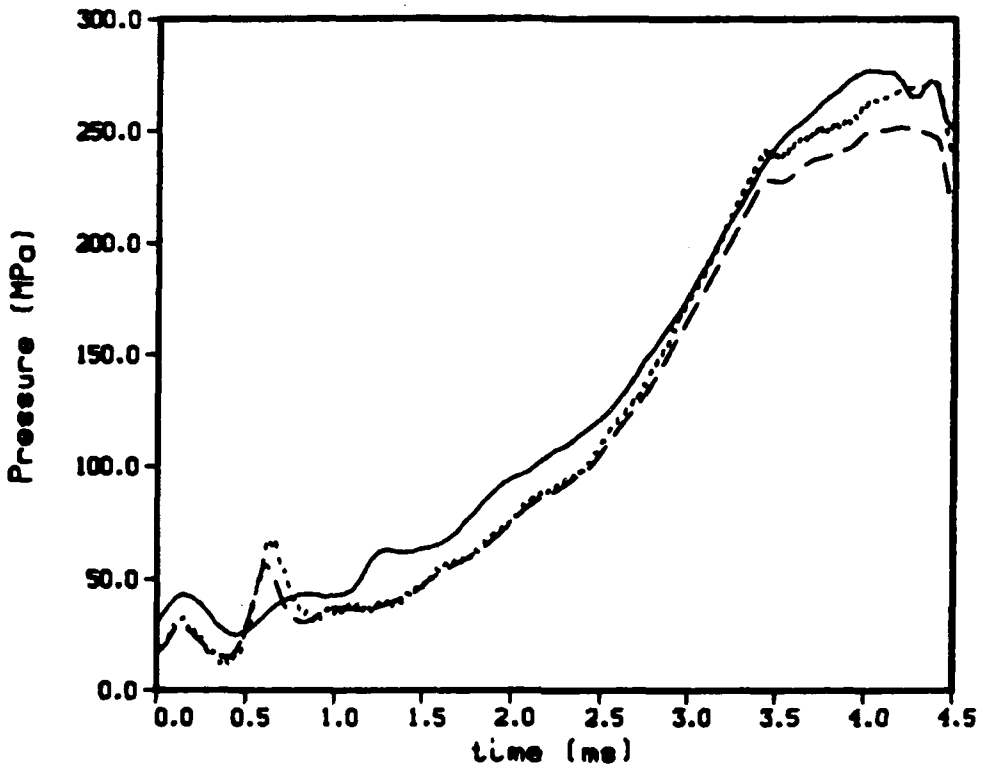

Figure 16. Back Wall Pressures
Round 8 (line).
ODIN Code (dot).
LPIN Code (dash).

The discharge coefficient is a useful correlation because it is a measure of the distance from steady state conditions. The pressure and velocity oscillations at the start of the firing cycle lead to very large oscillations in the discharge coefficient. A system without Belleville springs would generate cleaner profiles, since the initial oscillations in pressure and velocity would not be generated.

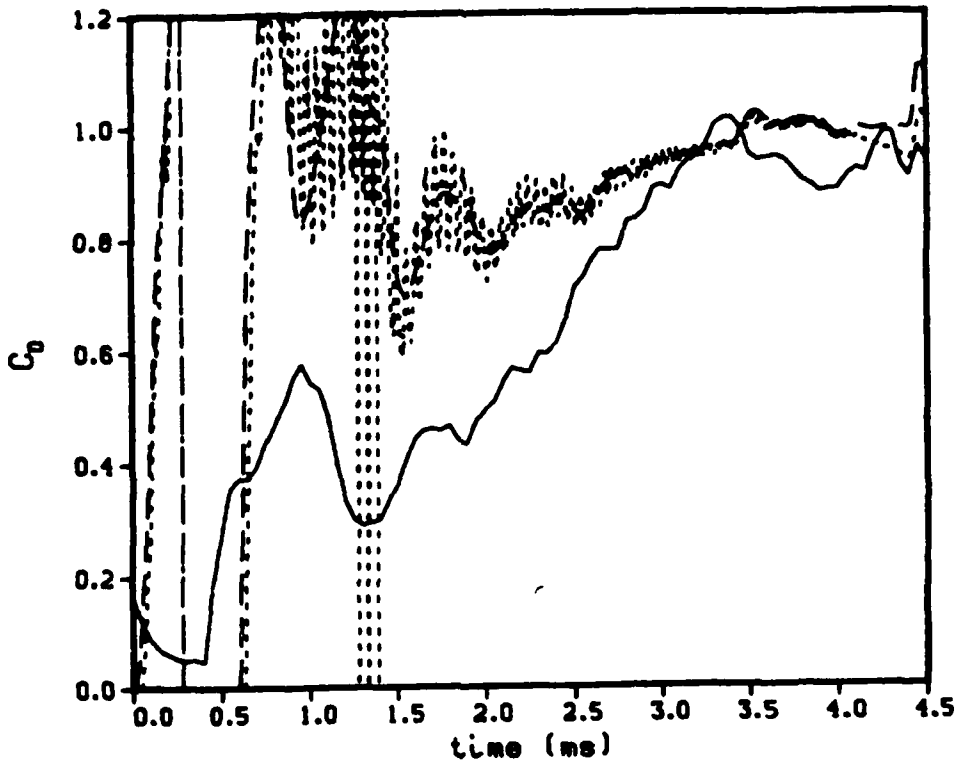

Figure 17. Discharge Coefficients
Round 8 (line).
ODIN Code (dot).
LPIN Code (dash).

The one-dimensional code does not include the effect of friction against the side walls. Friction should cause a higher liquid pressure and damp out the oscillations. Since this could lead to better agreement with the experiment, the effect of friction was examined using an empirical correlation. For fully developed turbulent flow in a cylinder of diameter D and length L, the head loss due to frictional effects is approximately[21]

$$\text{head loss} = \frac{.3164}{Re^{.25}} \frac{L}{D} \frac{u^2}{2} \qquad (14)$$

where u is the fluid velocity and Re is the Reynolds number. This gives a correction to the steady state Bernoulli equation. The head loss leads to a larger pressure difference from one end of the cylinder to the other. The correlation is applied to the velocity control volume. For the diameter of the cylinder the hydraulic diameter D_h = 2.0 x Gap is substituted. Adjusting the dimensions, the quantity

$$-\rho_J \frac{.3164}{Re^{.25}} \frac{\Delta x}{D_h} \frac{u_J^2}{2} \tag{15}$$

is added to equation (6), the finite difference form of the momentum equation. This gives an estimate to the effects of friction across the control volume.

The value of kinematic viscosity is 0.05 stokes.[13] Using the above correlation, the results are almost identical to the previous answers. Even if the kinematic viscosity is increased to 5.0 stokes, the differences are minor at the early times and only become important late in the cycle (see Figures 18-19). While the above approximation is crude, it should give the correct order of magnitude for frictional effects. The tentative conclusion is that for these high velocities and relatively low viscosities, frictional effects are not very important. When the MAGIC code is fully operational, this conclusion will be checked.

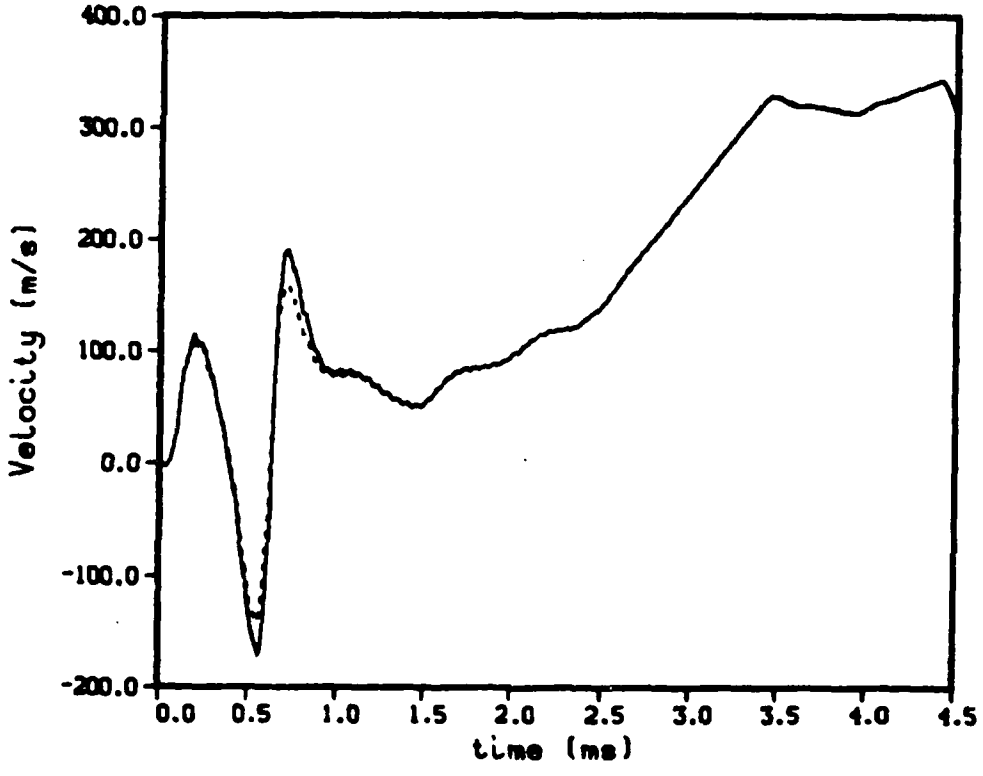

Figure 18. Outflux Fluid Velocities with Head Loss Correlation from ODIN Code.

ν = 0.0 (line).

ν = 5.0 (dot).

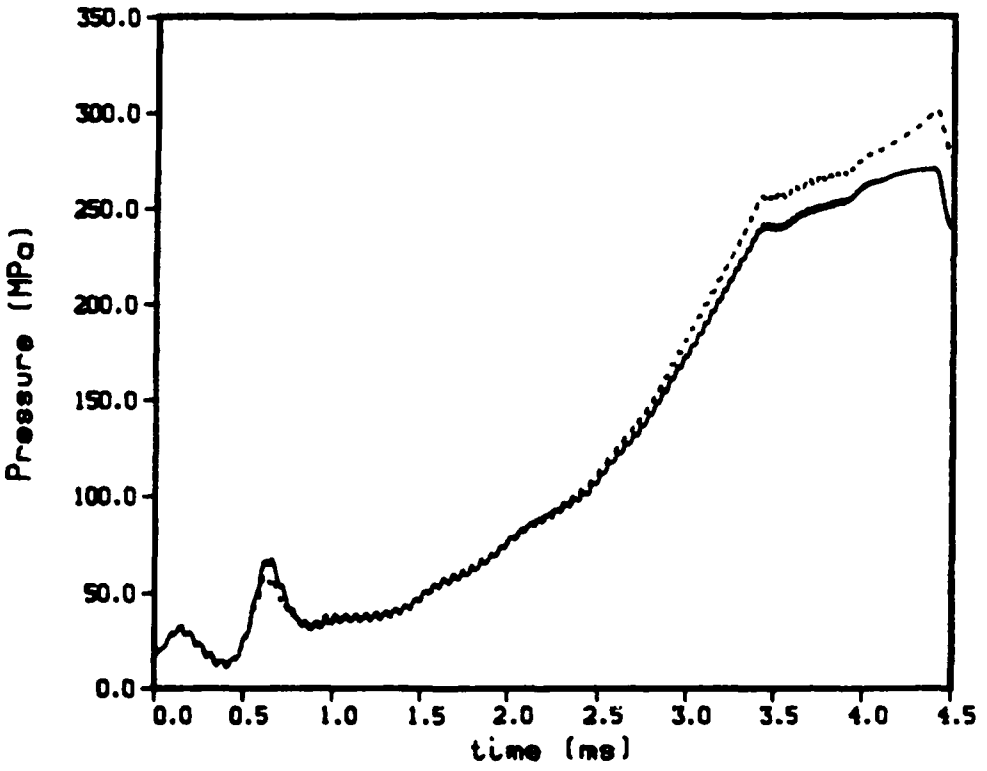

Figure 19. Back Wall Pressures with Head Loss Correlation from ODIN Code.

ν = 0.0 (line).

ν = 5.0 (dot).

X. CONCLUSIONS

Three models (lumped parameter, one-dimensional, and two-dimensional) have been developed for the injection of liquid propellant in a regenerative gun. For a simple test case, the models show reasonable agreement. For the actual gun simulation, only the two simpler models can be run. They both predict a rapid rise to roughly a steady state discharge coefficient. The results do not agree with values for the discharge coefficient obtained from the experimental data. Preliminary indications are that the two-dimensional model will give similar results. However, the development of the two-dimensional model should help to delineate the limitations of the one-dimensional analysis.

In conclusion, there is some phenomenon in the injection process which is not properly taken into account. The modeling of the liquid behavior may be perfectly adequate, and the problems due to other parts of the system. For example, the chamber pressure is assumed to be uniform, and the pressure measured at the wall is taken to be equal to the pressure at the exit of the reservoir. This is a boundary condition for the injection models considered here. If there is a noticeable pressure gradient in the chamber, this condition will be incorrect. Another possibility is the piston motion. The velocity of the piston is another boundary condition, and the position of the piston determines the shape of the liquid reservoir. If the piston wobbles about the central bolt, this will effect the injection area. The Belleville springs may have a more complicated behavior than than assumed, which would effect the measured position of the piston. Also, the piston travel measurements have ignored the effect of the recoil of the gun. These and other possible contributions to the piston motion are being investigated.

REFERENCES

1. Morrison, W.F., Knapton, J.D., and Klingenberg, G., "Liquid Propellants for Gun Applications," Proceedings of the Seventh International Symposium on Ballistics, The Hague, The Netherlands, April 1983.

2. Pagan, G. and Izod, D.C.A., "Regenerative Liquid Propellant Gun Modelling," Proceedings of the Seventh International Symposium on Ballistics, The Hague, The Netherlands, April 1983.

3. Cushman, P.G., "Regenerative Liquid Propellant Gun Simulation User's Manual," GE Report 84-POD-004, December 1983.

4. Gough, P.S., "A Model of the Interior Ballistics of Hybrid Liquid-Propellant Guns," Final Report, Contract DAAK11-82-C-1054, PGA-TR-83-4, September 1983.

5. Coffee, T.P., "A Lumped Parameter Code for Regenerative Liquid Propellant Guns," BRL-TR-2703, December 1985.

6. Coffee, T.P., "The Analysis of Experimental Measurements for Liquid Regenerative Guns," Technical Report BRL-TR-2731, May 1986.

7. Coffee, T.P., "Injection Processes in Liquid Regenerative Propellant Guns," BRL Technical Report, to be published.

8. Traci, R.M., "MAGIC Code", sections in Comparisons Between Measurement and Analysis of Fluid Motion in Internal Combustion Engine, Edit by P.D. Witzer, SAND81-8242, Sandia National Laboratories, Livermore, CA, 1981.

9. "MAGIC Report Draft," SAIC.

10. Phillips, G., Murty, S., Traci, R., and Edelman, R.B., "Analysis of Interior Ballistics Processes of Bulk Loaded Liquid Propellant Guns," 17th JANNAF Combustion Meeting, Vol. III, pp. 403-448, 1980, CPIA Publication 329.

11. Ramshaw, J.D. and Dukowicz, J.K., "APACHE: A Generalized-Mesh Eulerian Computer Code for Multicomponent Chemically Reactive Fluid Flow," Los Alamos Report LA-7427, January 1979.

12. Cloutman, L.D., Dukowicz, J.K., Ramshaw, J.D., and Andsden, A.A., CONCHAS-SPRAY: A Computer Code for Reactive Flows with Fuel Sprays," Los Alamos Report LA-9294-MS, May 1982.

13. Messina, N.A., Tseng, H.H., Ingram, L.S., and Summerfield, M., "The Role of Physical Properties in Dynamic Loading Processes and Bubble Collapse of Liquid Monopropellants for LPG Application," 21st JANNAF Combustion Meeting, Laurel, MD, October 1984.

14. Freedman, E., private communication, 1986.

15. Constantino, M., "The High Pressure Equation of State of LGP 1845 and LGP 1846 (U)," UCRL-93985 preprint, Aug. 1986. Submitted to the 1986 JANNAF Propulsion Meeting.

16. Roache, Patrick J., Computational Fluid Dynamics, pp. 64-67, Hermosa Publishers, 1972.

17. Roache, Patrick J., Computational Fluid Dynamics, pp. 228-230, Hermosa Publishers, 1972.

18. Reever, K. P., "Operating Manual and Final Test Report for 30-mm BRL Regenerative Liquid Propellant Test Fixture," General Electric Contract Report No. DAAK 11-83-C-0007.

19. Chu, C.K. and Sereny, A., "Boundary Conditions in Finite Difference Fluid Dynamic Codes," Journal of Computational Physics, Vol. 15, pp. 476-491, 1974.

20. Roache, Patrick J., Computational Fluid Dynamics, pp. 237-239, Hermosa Publishers, 1972.

21. Fox, R.W. and McDonald, A.T., Introduction to Fluid Mechanics, pp.359-365, John Wiley & Sons, 1985.

LIST OF SYMBOLS

a	speed of sound, cm/s.
A	cross-sectional area of liquid reservoir, cm^2.
C	Courant number.
C_D	discharge coefficient.
D_h	hydraulic diameter, cm.
g_o	conversion constant, 10 g/s^2-cm-MPa.
K	bulk modulus, MPa.
K_1	bulk modulus of the liquid at zero pressure, MPa.
K_2	derivative of the bulk modulus.
M	mass in a region, g.
p	pressure, MPa.
Re	Reynolds number ($u\ D_h/\nu$).
S	surface area, cm^2.
t	time, s.
u	fluid velocity, cm/s.
U	grid velocity, cm/s.

V	volume, cm^3.
ν	kinematic viscosity, stokes.
ρ_o	density of the liquid at atmospheric pressure, g/cm^3.
ρ	density of the liquid in the reservoir, g/cm^3.

DISTRIBUTION LIST

No. of Copies	Organization
12	Commander Defense Technical Info Center ATTN: DTIC-DDA Cameron Station Alexandria, VA 22304-6145
1	Director Defense Advanced Research Projects Agency ATTN: H. Fair 1400 Wilson Boulevard Arlington, VA 22209
1	HQDA DAMA-ART-M Washington, DC 20310
1	Commander US Army Materiel Command ATTN: AMCDRA-ST 5001 Eisenhower Avenue Alexandria, VA 22333-0001
13	Commander Armament R&D Center US Army AMCCOM ATTN: SMCAR-TSS SMCAR-TDC SMCAR-SCA, B. Brodman R. Yalamanchili SMCAR-AEE-B, D. Downs A. Beardell SMCAR-LCE, N. Slagg SMCAR-AEE-B, W. Quine A. Bracuti J. Lannon SMCAR-CCH, R. Price SMCAR-FSS-A, L. Frauen SMCAR-FSA-S, H. Liberman Picatinny Arsenal, NJ 07806-5000
3	Director Benet Weapons Laboratory Armament R&D Center US Army AMCCOM ATTN: SMCAR-LCB-TL E. Conroy A. Graham Watervliet, NY 12189
1	Commander US Army Armament, Munitions and Chemical Command ATTN: SMCAR-ESP-L Rock Island, IL 61299-7300
1	Commander US Army Aviation Research and Development Command ATTN: AMSAV-E 4300 Goodfellow Blvd St. Louis, MO 63120
1	Commander Materials Technology Lab US Army Laboratory Cmd ATTN: SLCMT-MCM-SB M. Levy Watertown, MA 02172-0001
1	Director US Army Air Mobility Rsch and Development Lab Ames Research Center Moffett Field, CA 94035
1	Commander US Army Communications Electronics Command ATTN: AMSEL-ED Fort Monmouth, NJ 07703

DISTRIBUTION LIST

No. of Copies	Organization
1	Commander ERADCOM Technical Library ATTN: STET-L Ft. Monmouth, NJ 07703-5301
1	Commander US Army Harry Diamond Labs ATTN: SLCHD-TA-L 2800 Powder Mill Rd Adelphi, MD 20783
1	Commander US Army Missile Command Rsch, Dev, & Engr Ctr ATTN: AMSMI-RD Redstone Arsenal, AL 35898
1	Commander US Army Missile & Space Intelligence Center ATTN: AIAMS-YDL Redstone Arsenal, AL 35898-5500
1	Commander US Army Belvoir R&D Ctr ATTN: STRBE-WC Tech Library (Vault) B-315 Fort Belvoir, VA 22060-5606
1	Commander US Army Tank Automotive Cmd ATTN: AMSTA-TSL Warren, MI 48397-5000
1	Commander US Army Research Office ATTN: Tech Library PO Box 12211 Research Triangle Park, NC 27709-2211

No. of Copies	Organization
1	Director US Army TRADOC Systems Analysis Activity ATTN: ATAA-SL White Sands Missile Range NM 88002
1	Commandant US Army Infantry School ATTN: ATSH-CD-CSO-OR Fort Benning, GA 31905
1	Commander Armament Rsch & Dev Ctr US Army Armament, Munitions and Chemical Command ATTN: SMCAR-CCS-C, T Hung Picatinny Arsenal, NJ 07806-5000
1	Commandant US Army Field Artillery School ATTN: ATSF-CMW Ft Sill, OK 73503
1	Commandant US Army Armor Center ATTN: ATSB-CD-MLD Ft Knox, KY 40121
1	Commander US Army Development and Employment Agency ATTN: MODE-TED-SAB Fort Lewis, WA 98433
1	Commander Naval Surface Weapons Center ATTN: D.A. Wilson, Code G31 Dahlgren, VA 22448-5000
1	Commander Naval Surface Weapons Center ATTN: Code G33, J. East Dahlgren, VA 22448-5000

DISTRIBUTION LIST

No. of Copies	Organization
2	Commander US Naval Surface Weapons Ctr ATTN: O. Dengel K. Thorsted Silver Spring, MD 20902-5000
1	Commander Naval Weapons Center China Lake, CA 93555-6001
1	Commander Naval Ordnance Station ATTN: C. Dale Code 5251 Indian Head, MD 20640
1	Superintendent Naval Postgraduate School Dept of Mechanical Engr ATTN: Code 1424, Library Monterey, CA 93943
1	AFWL/SUL Kirtland AFB, NM 87117
1	Air Force Armament Lab ATTN: AFATL/DLODL Eglin AFB, FL 32542-5000
1	AFOSR/NA (L. Caveny) Bldg 410 Bolling AFB, DC 20332
1	Commandant USAFAS ATTN: ATSF-TSM-CN Ft Sill, OK 73503-5600
1	US Bureau of Mines ATTN: R.A. Watson 4800 Forbes Street Pittsburgh, PA 15213
1	Director Jet Propulsion Lab ATTN: Tech Library 4800 Oak Grove Drive Pasadena, CA 91109
2	Director National Aeronautics and Space Administration ATTN: MS-603, Tech Lib MS-86, Dr. Povinelli 21000 Brookpark Road Lewis Research Center Cleveland, OH 44135
1	Director National Aeronautics and Space Administration Manned Spacecraft Center Houston, TX 77058
10	Central Intelligence Agency Office of Central Reference Dissemination Branch Room GE-47 HQS Washington, DC 20502
1	Central Intelligence Agency ATTN: Joseph E. Backofen HQ Room 5F22 Washington, DC 20505
3	Bell Aerospace Textron ATTN: F. Boorady F. Picirillo A.J. Friona PO Box One Buffalo, NY 14240
1	Calspan Corporation ATTN: Tech Library PO Box 400 Buffalo, NY 14225

DISTRIBUTION LIST

No. of Copies	Organization
7	General Electric Ord Sys Div ATTN: J. Mandzy, OP43-220 R.E. Mayer H. West M. Bulman R. Pate I. Magoon J. Scudiere 100 Plastics Avenue Pittsfield, MA 01201-3698
1	General Electric Company Armament Systems Department ATTN: D. Maher Burlington, VT 05401
1	IITRI ATTN: Library 10 W. 35th St Chicago, IL 60616
1	Olin Chemicals Research ATTN: David Gavin PO Box 586 Chesire, CT 06410-0586
2	Olin Corporation ATTN: Victor A. Corso Dr. Ronald L. Dotson PO Box 30-9644 New Haven, CT 06536
1	Paul Gough Associates ATTN: Paul Gough PO Box 1614 Portsmouth, NH 03801
1	Safety Consulting Engr ATTN: Mr. C. James Dahn 5240 Pearl St Rosemont, IL 60018
3	Science Applications, Inc. ATTN: R. Edelman 23146 Cumorah Crest Woodland Hills, CA 91364
1	Sundstrand Aviation Operations ATTN: Mr. Owen Briles PO Box 7202 Rockford, IL 61125
1	Veritay Technology, Inc. ATTN: E.B. Fisher 4845 Millersport Highway PO Box 305 East Amherst, NY 14051-0305
1	Director Applied Physics Laboratory The Johns Hopkins Univ. Johns Hopkins Road Laurel, MD 20707
2	Director CPIA The Johns Hopkins Univ. ATTN: T. Christian Tech Library Johns Hopkins Road Laurel, MD 20707
1	U. of Illinois at Chicago ATTN: Professor Sohail Murad Dept of Chemical Engr Box 4348 Chicago, IL 60680
1	U. of MD at College Park ATTN: Professor Franz Kasler Department of Chemistry College Park, MD 20742

DISTRIBUTION LIST

No. of Copies	Organization
1	U. of Missouri at Columbia ATTN: Professor R. Thompson Department of Chemistry Columbia, MO 65211
1	U. of Michigan ATTN: Prof. Gerard M. Faeth Dept of Aerospace Engr Ann Arbor, MI 48109-3796
1	U. of Missouri at Columbia ATTN: Professor F.K. Ross Research Reactor Columbia, MO 65211
1	U. of Missouri at Kansas City Department of Physics ATTN: Prof. R.D. Murphy 1110 East 48th Street Kansas City, MO 64110-2499
1	Pennsylvania State University Dept of Mechanical Engr ATTN: Prof. K. Kuo University Park, PA 16802
2	Princeton Combustion Rsch Laboratories, Inc. ATTN: N.A. Messina M. Summerfield 475 US Highway One North Monmouth Junction, NJ 08852
1	University of Arkansas Dept of Chemical Engr ATTN: J. Havens 227 Engineering Building Fayetteville, AR 72701
3	University of Delaware Department of Chemistry ATTN: Mr. James Cronin Professor Thomas Brill Mr. Peter Spohn Newark, DE 19711

Aberdeen Proving Ground

Dir, USAMSAA
ATTN: AMXSY-D
AMXSY-MP, H. Cohen

Cdr, USATECOM
ATTN: AMSTE-TO-F

Cdr, CRDEC, AMCCOM
ATTN: SMCCR-RSP-A
SMCCR-MU
SMCCR-SPS-IL

USER EVALUATION SHEET/CHANGE OF ADDRESS

This Laboratory undertakes a continuing effort to improve the quality of the reports it publishes. Your comments/answers to the items/questions below will aid us in our efforts.

1. BRL Report Number_____ Date of Report_____

2. Date Report Received_____

3. Does this report satisfy a need? (Comment on purpose, related project, or other area of interest for which the report will be used.)_____

_____

_____

4. How specifically, is the report being used? (Information source, design data, procedure, source of ideas, etc.)_____

_____

_____

5. Has the information in this report led to any quantitative savings as far as man-hours or dollars saved, operating costs avoided or efficiencies achieved, etc? If so, please elaborate._____

_____

_____

6. General Comments. What do you think should be changed to improve future reports? (Indicate changes to organization, technical content, format, etc.)

_____

_____

_____

CURRENT ADDRESS

_____
Name

_____
Organization

_____
Address

_____
City, State, Zip

7. If indicating a Change of Address or Address Correction, please provide the New or Correct Address in Block 6 above and the Old or Incorrect address below.

OLD ADDRESS

_____
Name

_____
Organization

_____
Address

_____
City, State, Zip

(Remove this sheet, fold as indicated, staple or tape closed, and mail.)

FOLD HERE

Director
US Army Ballistic Research Laboratory
ATTN: DRXBR-OD-ST
Aberdeen Proving Ground, MD 21005-5066

NO POSTAGE
NECESSARY
IF MAILED
IN THE
UNITED STATES

OFFICIAL BUSINESS
PENALTY FOR PRIVATE USE, $300

BUSINESS REPLY MAIL
FIRST CLASS PERMIT NO 12062 WASHINGTON, DC
POSTAGE WILL BE PAID BY DEPARTMENT OF THE ARMY

Director
US Army Ballistic Research Laboratory
ATTN: DRXBR-OD-ST
Aberdeen Proving Ground, MD 21005-9989

FOLD HERE

END

DATE

FILMED

8-88

DTIC